Density Functional Study of the Effect of SiH_4/GeH_4 and Si(001)/Ge(001) on Gas-Surface Reactivity during Initial Dissociative Adsorption

Jyh Shing Lin* (林志興), Lien-Feng Lee (李連峰) and Wen-Chi Chou (周文祺)
Department of Chemistry, Tamkang University, Tamsui, Taiwan 25137, R.O.C.

Ultrasoft pseudopotential total energy calculation based on density functional theory (DFT) with generalized gradient approximation (GGA) has been used to investigate 1) the energetic profile for the initial dissociative adsorption of XH_4 (X = Si and Ge) onto Si(001) and Ge(001) surfaces to evaluate their gas-surface reactivity in comparison with relevant measured gas-surface reactivity using supersonic molecular beam techniques, and 2) the effect of different gaseous molecular precursors, i.e. XH_4 (X = Si and Ge), and different surfaces, i.e. Si(001) and Ge(001), on their gas-surface reactivity during initial dissociative adsorption. Our evaluated gas-surface reactivity for GeH_4 is approximately a factor of 18.45 better than that for SiH_4 on Si(001)-(2×2) surface. This calculated result is about three to four times higher than observed gas-surface reactivity (as much as a factor of 5 depending on the incident kinetic energy) derived from measured gas-surface reactivity using supersonic molecular beam techniques. We believe that the better evaluated gas-surface reactivity for GeH_4 than SiH_4 is due to 1) the forming of a stronger bond of Si-H between H within GeH_4 and buckled-down Si atom on the Si(001)-(2×2) surface and 2) the smaller distortion of Ge-H bond within GeH_4 at the transition state. Additionally, our evaluated gas-surface reactivity for SiH_4 on Si(001)-(2×2) surface is approximately a factor of 21.69 better than SiH_4 on Ge(001)-(2×2) surface. This calculated result is about two times higher than observed gas-surface reactivity. We attributed this better evaluated gas-surface reactivity for SiH_4 on Si(001)-(2×2) surface to 1) the smaller distortion of Si-H bond within SiH_4 and 2) the nature of weaker bond of Ge-H between H within SiH_4 and buckled-down Ge atom on Ge(001)-(2×2) surface in comparison with that of stronger bond of Si-H between H within SiH_4 and buckled-down Si atom on Si(001)-(2×2) surface even though there is the slightly shorter bond length of Ge-H between H within SiH_4 and buckled-down Ge atom on Ge(001)-(2×2) surface at the transition state.

Keywords: Silane; Germane; Silicon surface; Germanium surface; Ultrasoft Pseudopotential; Density functional theory.

INTRODUCTION

Consistent with the increasing demand of shrinking electronic devices, it is of crucial importance to manipulate the fabrication process on the microscopic level. Recent interest in epitaxial growth of both Si and Ge thin films has been sparked by the $Si_{1-x}Ge_x$ alloys,[1-3] which are employed both in bandgap engineering possibilities and in heterojunction bipolar transistors.[4] These $Si_{1-x}Ge_x$ layers on silicon and germanium substrates are routinely grown from mixed gaseous precursors by a variety of chemical vapor deposition (CVD) processes,[4-9] and silane (SiH_4 and Si_2H_6) and germane (GeH_4 and Ge_2H_6), are the most common CVD gaseous precursors. During the last decade supersonic molecular beam techniques[10-12] have been employed by Engstrom and his co-worker to examine the initial dissociative adsorption of GeH_4 and SiH_4 onto both Si(001) and Ge(001) surfaces leading to the formation of Si(001)(SiH_3:H and GeH_3:H) and Ge(001)(SiH_3:H and GeH_3:H). It has been observed from their experimental data that the difference in gas-surface reactivity depends on the chemical identity of the thin film precursor, the incident kinetic energy and the substrate temperature. At comparable incident kinetic energies and substrate temperatures, the GeH_4 is more reactive (a factor of between 2 and 5 depending on the incident kinetic energy) than its Si counterpart on Si(001) surface. Additionally, it is found that both Si(001) and Si(111) surfaces are much more reactive (as much as a factor of 10 depending on the incident kinetic energy) than their Ge counterparts in terms of initial dissociative adsorption of SiH_4 onto these surfaces. These experimental observations prompt us for this study using ultrasoft pseudopotential total energy calculation in connection with den-

Special Issue for the Second Worldwide Chinese Theoretical and Computational Chemistry Conference

sity functional theory and periodic slab model to evaluate their gas-surface reactivity for the initial dissociative adsorption of GeH_4 and SiH_4 onto both Si(001) and Ge(001) surfaces. In particular, the increasing growth rate of $Si_{1-x}Ge_x$ alloys is due to the increased gas-surface reactivity of thin film precursors on both Si(001) and Ge(001) surfaces. Therefore, knowledge of their gas-surface reactivity on the microscopic level is crucial for developing predictive models for $Si_{1-x}Ge_x$ film growth relating the incident flux of the precursors to the resulting bulk Ge composition and the surface composition of Ge, which in general will be different. Without doubt these calculated results should provide the experimental guide for choosing different incident kinetic energies of different gaseous molecular precursors and different substrate temperatures for better control of thin film growth of $Si_{1-x}Ge_x$ during the CVD process.

Only a few theoretical studies of the initial dissociative adsorption of SiH_4 onto Si(001)-(2×1) surface have been reported. For example, Kang and Musgrave, using density functional theory with generalized gradient approximation and five-layer $Si_{23}H_{24}$ two-dimer trench cluster, investigate the chemical vapor of Si(001) from silane deposition.[36] Katircioglu and Erokc, using density functional method in connection with a surface model of $Si_{19}H_{20}$ cluster to explore the mechanism of dissociative adsorption of silane on the S_A type stepped Si(001) surface.[37] Brown and Doren,[13] using density functional method with generalized gradient approximation and a surface model of the Si_9H_{12} cluster, explored the mechanism of dissociative adsorption of SiH_4 onto Si(001)-(2×1) surface with no symmetry and geometric constraints. Jing and Whitten,[14] using configuration interaction methods and a surface model of $Si_{19}H_{21}$ cluster, located a transition state without following the reaction path to products. To my knowledge, the work on initial dissociative adsorption of SiH_4 and GeH_4 onto both Si(001) and Ge(001) surfaces has not previously been studied with a periodic boundary condition method except for our works[15-16,38] using *ab initio* norm-conserving pseudopotential total energy calculations with generalized gradient approximation (GGA) successfully to establish structural and energetic characteristic of silane initial dissociative adsorption onto Si(001) and Si(111) surfaces. Therefore, in this work we employed very similar *ab initio* ultrasoft pseudopotential[28,35] total energy calculations with generalized gradient approximation (GGA) and partial structural constraint path minimization method to mainly focus on 1) the energetic profiles associated with the process of the initial dissociative adsorption of SiH_4 and GeH_4 onto both Si(001) and Ge(001) surfaces in order to evaluate their gas-surface reactivity and 2) the effect of different gaseous molecular precursors, i.e. XH_4 (X = Si and Ge), and different surfaces, i.e. Si(001) and Ge(001), on their gas-surface reactivity during initial dissociative adsorption process in order to rationalize the factors dictating their gas-surface reactivity in comparison with the measured gas-surface reactivity using supersonic molecular beam techniques.

COMPUTATIONAL METHODS

Density functional theory[17] (DFT) with generalized gradient approximation (GGA) is applied to perform the *ab initio* total energy ultrasoft pseudopotential calculations.[18-20] Our computational strategy is to perform all the calculations using periodic boundary conditions, sometimes known as the supercell method, with the electronic orbital represented by using a plane-wave basis set. We have used the density mixing scheme described by Kresse and Furthmuller[21] to efficiently reach self-consistency for the Kohn-Sham energy functional in which GGA of Perdew and Wang,[22] implemented as described by White and Bird,[23] is utilized. For the Brillouin-zone integration we used a 2×2×1 grid of Monkhorst-Pack special points[24] after the convergence test of energetic data of Si(001)-(2×2) with a grid of 3×3×1. We also explored the plane-wave convergence test by calculating the structural parameter of H_3Si-H, i.e. bond length of Si-H within SiH_4, and dissociative adsorption energy of SiH_4 adsorbed on the Si(001)-(2×2) surface as reported in Table 1. Our calculated bond length of Si-H with a cut-off of 200 eV is 0.002 Å different from that of 250 eV, and our calculated adsorption energy of SiH_4 adsorbed on the Si(001)-(2×2) with a cut-off of 200 eV is only 0.005 eV different from that of 250 eV. These results clearly demonstrate that the energy cut-off of 200 eV is

Table 1. Energy Cut-off Tests for the Bond Length of Si-H within SiH_4 and the Adsorption Energy of SiH_4 Adsorbed on the Si(001)-(2×2) Surface

Energy cut-off (eV)	Si-H bond length (Å)
150	1.485
200	1.478
250	1.476
Expt.	1.480
Energy cut-off (eV)	E_{ads}
150	1.993
200	1.952
250	1.947

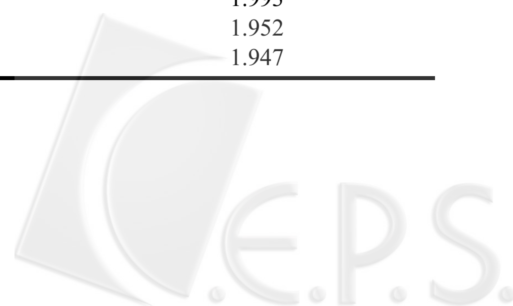

adequate for the calculated physical and chemical properties of our interest in this study. In our calculations both Si(001) and Ge(001) are represented by Si(001)-(2×2) and Ge(001)-(2×2) surface models, respectively, and were constructed by a periodically repeated slab of Si and Ge atoms (six layers in the unreconstructed geometry), respectively, with one side of three layers fixed and the other side of three layers followed by a vacuum region of approximately 13 Å. These vacuum layers are mainly introduced to avoid the interaction between surfaces due to the periodicity along the [001] direction. In addition, the dangling bonds on the side of the fixed layers were passivated by an H atom to eliminate the charge sloshing effect between the two surfaces.

In our previous work[15-16,38] the pseudopotential of silicon was constructed based on the standard Kerker[25] method of pseudopotential generation with the conditions of norm conservation[26-27] and continuity of the wavefunction and its first and second derivatives at the core radius. The norm conservation condition is thought to improve the transferability of the pseudopotential. Also, by increasing the core radius can soften the pseudopotential, but the loss of accuracy and transferability puts an upper limit to core radius and hence to a further reduction of the plane-wave basis set. Recently, Vanderbilt[28,35] pointed out that the main obstacle to a further increase of core radius is the requirement of the norm conservation condition to improve the transferability. Therefore, he introduces what is called "ultrasoft pseudopotential" to improve the transferability by fitting not just one, but at least at two reference energies and to use a small set of localized "augmenation functions" to describe the charge density deficit arising from the violation of the norm conservation condition. In consequence, the core radius can be increased to some extent without sacrificing their transferability. In addition, a Kleinman-Bylander representation[29] of the ultrasoft pseudopotential is automatically introduced due to the nature of its construction. This allows the plane-wave matrix elements for the ultrasoft pseudopotential to be expressed in a separable form for computational efficiency.

For the ultrasoft pseudopotential of Si it is generated with an atomic reference electron-configuration $3s^2 3p^2$ of core radii $r_{c,s} = r_{c,p} = 0.952$ Å, augmentation radii of $r_{aug,s} = 0.688$ Å and $r_{aug,p} = 0.688$ Å for the construction of the pseudized augmentation functions and reference energies of $\varepsilon_{s,1} = -19.047$ eV, $\varepsilon_{s,2} = 6.803$ eV, $\varepsilon_{p,1} = -11.700$ eV and $\varepsilon_{p,2} = 6.803$ eV. The d-component of Si pseudopotential is simply generated in such a way that it matches smoothly around the core radius of 0.952 Å to the screened potential which is constructed by carrying out all-electron calculation on a free Si atom in the same reference configuration and is chosen to be the local for the Kleinman-Bylander representation. For the ultrasoft pseudopotential of Ge it is generated with an atomic reference electron-configuration $4s^2 4p^2$ of core radii $r_{c,s} = r_{c,p} = 1.217$ Å, augmentation radii of $r_{aug,s} = 0.794$ Å and $r_{aug,p} = 0.794$ Å for the construction of the pseudized augmentation functions and reference energies of $\varepsilon_{s,1} = -11.972$ eV, $\varepsilon_{s,2} = 6.803$ eV, $\varepsilon_{p,1} = -4.082$ eV and $\varepsilon_{p,2} = 6.803$ eV. The d-component of the Ge pseudopotential is generated in a similar way to match smoothly around the core radius of 1.217 Å to the screened potential which is constructed by carrying out all-electron calculation on a free Ge atom in the same reference configuration and is chosen to be the local for the Kleinman-Bylander representation. Although Si and Ge pseudopotentials are constructed using only local density approximation (LDA), it has shown to be highly transferable over the required energy ranges from neutral atoms,[30] dimers,[31] silicon oxide defects,[31] and silicon surface reconstruction.[32] For the ultrasoft pseudopotential of H it is generated with an atomic reference electron configuration $1s^1$ of core radius $r_{c,s} = 0.423$ Å, augmentation radius of $r_{aug,s} = 0.423$ Å for the construction of the pseudized augmentation function and reference energy of $\varepsilon_{s,1} = -6.394$ eV. Another s-component of the H pseudopotential is generated in a similar way to match smoothly around the core radius 0.423 Å to the screened potential which is constructed by carrying out all-electron calculation on free Si atom in the same reference configuration and is chosen to be the local for the Kleinman-Bylander representation.

Finally, the activation energy calculation for both SiH_4 and GeH_4 initial dissociative adsorption onto both Si(001)-(2×2) and Ge(001)-(2×2) surfaces requires that the saddle point, i.e. transition state, be identified. This is generally straightforward by using the energy minimization method of partial structural constraint path leading from reactant, i.e. both SiH_4 and GeH_4 above Si(001)-(2×2) and Ge(001)-(2×2) surfaces, to the saddle point, i.e. transition state, and finally to the products i.e. Si(001)-(2×2)(SiH_3:H and GeH_3:H) and Ge(001)-(2×2)(SiH_3:H and GeH_3:H). The details of this method are described in one our previous paper.[16] We performed all the total energy calculations using the modified version of CASTEP 3.9.[33]

CALCULATED RESULTS AND DISCUSSIONS

Surface structures of Si(001)-(2×2) and Ge(001)-(2×2)

Our previous studies[15,16] established that the relaxation

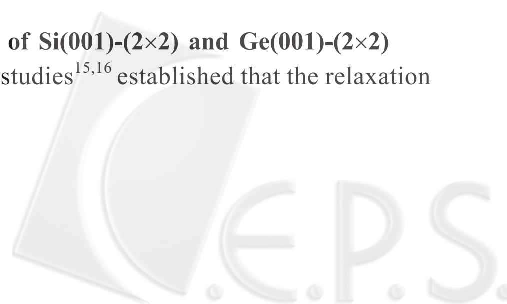

of a Si(001)-(2×2) surface leads to the formation of buckled Si=Si dimer with some π-bonding character in the buckled Si=Si dimer. In addition, the reconstruction of the Si(001)-(2×2) surface also leads to a slight contraction of the Si-Si distance between the first and second layers. The ultrasoft pseudopotential is used to replace the norm-conserving pseudopotential by taking advantage of using a smaller cut-off in our total energy calculations. Therefore, it is important to assure that the incorporation of the ultrasoft pseudopotential approximation should produce a very similar structural characteristic of the buckled Si=Si dimer of the Si(001)-(2×2) surface. Indeed, our calculated bond lengths of the buckled Si=Si dimer and corresponding buckling angles are consistent with our previous results as shown in Table 2. In addition, our calculated structural parameters are in reasonable agreement with other calculated results using the cluster model.[36,37] Detailed discussions of the structural properties of the relaxed Si(001) surface have been given in our previous studies.[15,16] The calculated structural parameters of Ge(001)-(2×2) as shown in Table 2 are also characterized by similar buckled and alternated Ge=Ge dimer, i.e. one dimer component is at the higher position than the other and neighboring dimers are titled in opposition. The buckling of the dimer allows charge from the buckled-down atom (which becomes more sp^2 bonded) to the buckled-up atom (which becomes more sp^3 bonded). Thus the buckled-up atom is electron rich but the buckled-down atom is electron deficient. Our calculated bond length and tilt angle of the Ge=Ge dimer are 2.482 Å and 18.0°, respectively, which are in good agreement with previous theoretical and experimental work.[39,40] Furthermore, to validate our calculated results using DFT-GGA plus ultrasoft pseudopotential we also calculated the bond lengths of H_2 and SiH_3-H and the lattice parameter of germanium bulk to validate our calculated results using DFT-GGA plus ultrasoft pseudopotential. Our calculated bond lengths of H_2 and SiH_3-H give 0.744 Å and 1.482 Å, respectively, in good agreement with experimental data and our calculated lattice parameter of germanium bulk is only 1.5% larger than the experimental parameter.

Table 2. Calculated Bond Lengths (Å) of Both Relaxed Buckled Si=Si Dimer on Si(001)-(2×2) Surface and Relaxed Buckled Ge=Ge Dimer on Ge(001)-(2×2) Surface. The d_{12} is the Average Distance between the Top Layer of Si and Ge, i.e. Si=Si Dimer and Ge=Ge Dimer, and Second Layer of Si and Ge. The d_{23} is the Average Distance between the Second Layer and Third Layer. The d_{34} is the Average Distance between the Third Layer and Fourth Layer. The Number in the Parenthese is from Ref. 16

	Relaxed buckled Si=Si dimer	Relaxed buckled Ge=Ge dimer
Si=Si dimer (1) (Å)	2.358 (2.355)	
Ge=Ge dimer (1) (Å)		2.482
Si=Si dimer (2) (Å)	2.318 (2.313)	
Ge=Ge dimer (2) (Å)		2.484
d_{12} (Si-Si) (Å)	2.346 (2.329)	
d_{12} (Ge-Ge) (Å)		2.458
d_{23} (Si-Si) (Å)	2.365 (2.382)	
d_{23} (Ge-Ge) (Å)		2.451
d_{34} (Si-Si) (Å)	2.356 (2.389)	
d_{23} (Ge-Ge) (Å)		2.434
Si=Si dimer (1) tilt (°)	18.1 (17.4)	
Ge=Ge dimer (1) tilt (°)		18.1
Si=Si dimer (2) tilt (°)	-15.9 (-15.6)	
Ge=Ge dimer (2) tilt (°)		-18.0

Geometrical Structures and Thermal Stabilities of Si(001)-(2×2)(SiH_3:H), Si(001)-(2×2)(GeH_3:H) and Ge(001)-(2×2)(SiH_3:H)

It has been suggested[7,12] that during the initial dissociative adsorption of SiH_4 and GeH_4 onto both Si(001)-(2×2) and Ge(001)-(2×2) surfaces, Si(001)-(2×2)(SiH_3:H and GeH_3:H) and Ge(001)-(2×2)(SiH_3:H and GeH_3:H) are the initial products. In this section we will first focus on the description of geometrical structures of Si(001)-(2×2)(SiH_3:H) and Si(001)-(2×2)(GeH_3:H) and their energetic data in order to rationalize the effect of different gaseous molecular precursors on their thermal stabilities of these initial products during the initial dissociative adsorption of SiH_4 and GeH_4 onto a Si(001)-(2×2) surface. Our calculated structures of Si(001)-(2×2)(SiH_3:H) and Si(001)-(2×2)(GeH_3:H) are shown in Fig. 1. The corresponding energetic data, i.e., dissociative adsorption energy, and the structural parameters are presented in Table 3(a). In order to validate this calculated energetic data using DFT-GGA plus ultrasoft pseudopotential we also calculated the bond strength of SiH_3-H. Our calculated bond strength of SiH_3-H gives 3.89 eV in good agreement with the experimental data (3.91 eV) of Walsh.[34]

From our calculated structural and energetic data we found that the buckled Si=Si dimer involving both SiH_4 and GeH_4 initial dissociative adsorption has a longer bond length and smaller tilt angle after dissociative adsorption. This is due to the change of Si on Si=Si dimer from sp^2 to sp^3 hybridization. But the buckled Si=Si dimer involving SiH_4 initial dissociative adsorption has an even longer bond length than that involving GeH_4 initial dissociative adsorption. We attribute this longer bond length to the formation of stronger

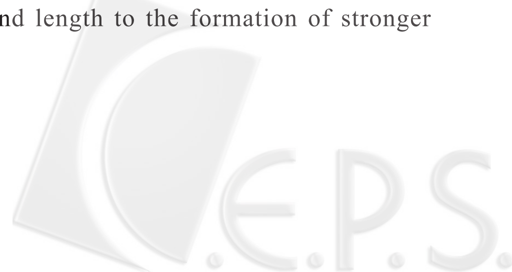

Table 3. (a) Calculated Bond Lengths (Å) and Bond Angles (°) of Both SiH_4 and GeH_4 Adsorbed Si(001)-(2×2) Surfaces, i.e., Si(001)-(2×2)(SiH_3:H) and Si(001)-(2×2)(GeH_3:H), and Corresponding Adsorption Energies E_{ads}. (b) Calculated Bond Lengths (Å) and Bond Angles (°) of Both SiH_4 and GeH_4 Adsorbed Ge(001)-(2×2) Surfaces, i.e., Ge(001)-(2×2)(SiH_3:H) and Ge(001)-(2×2)(GeH_3:H), and Corresponding Adsorption Energies E_{ads}

(a)	SiH_4 adsorbed Si(001)-(2×2)	GeH_4 adsorbed Si(001)-(2×2)
Si=Si dimer (1) (Å)	2.406	2.370
Si=Si dimer (2) (Å)	2.279	2.256
Si_d-H in SiH_4 (Å)	1.491	
Si_d-H in GeH_4 (Å)		1.490
Si_u-Si in SiH_4 (Å)	2.303	
Si_u-Ge in GeH_4 (Å)		2.348
Si=Si dimer (1) tilt (°)	0.4	1.3
Si=Si dimer (2) tilt (°)	-14.0	-14.9
$E_{ads.}$(eV)	1.993	2.036
(b)	**SiH_4 adsorbed Ge(001)-(2×2)**	**GeH_4 adsorbed Ge(001)-(2×2)**
Ge=Ge dimer (1) (Å)	2.458	2.452
Ge=Ge dimer (2) (Å)	2.435	2.433
Ge_d-H in SiH_4 (Å)	1.529	
Ge_d-H in GeH_4 (Å)		1.528
Ge_u-Si in GeH_4 (Å)	2.344	
Ge_u-Ge in GeH_4 (Å)		2.369
Ge=Ge dimer (1) tilt (°)	2.1	1.6
Ge=Ge dimer (2) tilt (°)	-17.0	-17.0
$E_{ads.}$(eV)	1.482	1.506

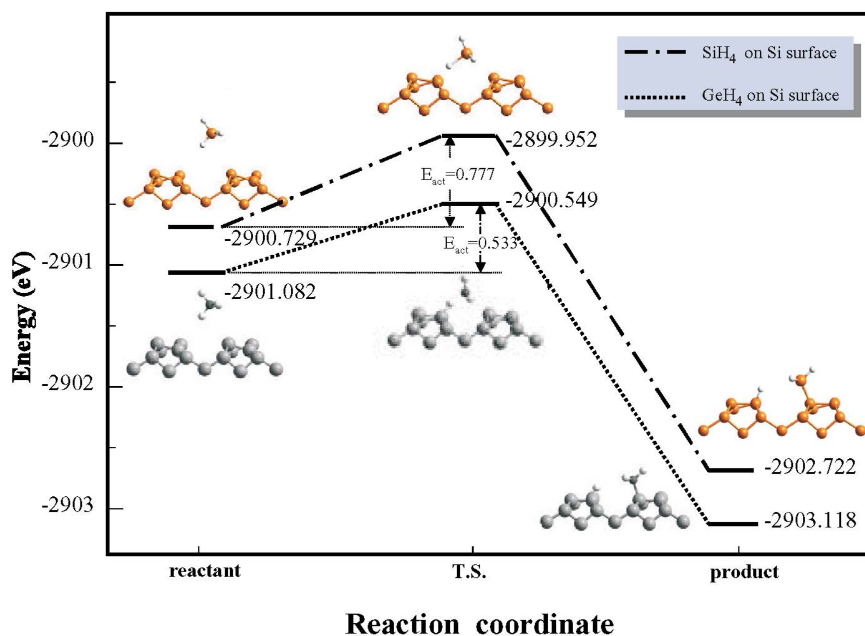

Fig. 1. Energy profiles following the partial structural constraint path of the initial dissociative adsorption of both SiH_4 and GeH onto a Si(001)-(2×2) surface and the corresponding structures. The reaction coordinate refers to the structural constraint of both Si-H and Ge-H bond lengths (Å) along the constraint path of the initial dissociative adsorption of both SiH_4 and GeH_4 onto the Si(001)-(2×2) surface as described in Ref. 16.

C.E.P.S.

Si-SiH_3 bond in comparison with Si-GeH_3 bond thereby weakening the π character of the buckled Si=Si dimer. On the other end, the other buckled Si=Si dimer has a shorter bond length after initial dissociative adsorption. This is due to the fact that the effect of the surface electronic states of the buckled Si=Si dimer involving both SiH_4 and GeH_4 initial dissociative adsorption on that of the other buckled Si=Si dimer becomes less important after both SiH_4 and GeH_4's initial dissociative adsorption. Consequently, this buckled Si=Si dimer will behave as an independent buckled Si=Si dimer to allow the enhancement of the buckled Si=Si bond strength, i.e. the decrease of bond length. Finally, our calculated dissociative adsorption energies of both SiH_4 and GeH_4 on the Si(001)-(2×2) are 1.993 eV and 2.036 eV, respectively. These results indicate that both SiH_4 and GeH_4's initial dissociative adsorption onto the Si(001)-(2×2) surface are energetically favorable and they lead to the formation Si(001)-(2×2)(SiH_3:H) and Si(001)-(2×2)(GeH_3:H), respectively. To further explore the effect of different surfaces, i.e. Si(001)-(2×2) and Ge(001)-(2×2), on the stability of both Si(001)-(2×2)(SiH_3:H) and Ge(001)-(2×2)(SiH_3:H) during the initial dissociative adsorption of SiH_4 onto both Si(001)-(2×2) and Ge(001)-(2×2) surfaces, the geometrical structure of Ge(001)-(2×2)(SiH_3:H) has also been calculated and is shown in Fig. 2. The corresponding energetic data, i.e., dissociative adsorption energy, and the structural parameters are presented in Table 3(b). Indeed, the characteristics of both surface structures, i.e. Si(001)-(2×2)(SiH_3:H) and Ge(001)-(2×2)(SiH_3:H), based on our calculated results are very similar. In consequence, the initial dissociative adsorption of SiH_4 onto the Ge(001)-(2×2) surface is energetically favorable but the calculated dissociative adsorption energies is around 0.5 eV smaller than its Si counterpart. We attributed these smaller dissociative adsorption energies to the weaker bond of Ge-H between H within SiH_4 and buckled-down Ge atom on one buckled Ge=Ge dimer and that of Ge-SiH_3 between SiH_3 fragment within SiH_4 and buckled-up Ge atom on an adjacent buckled Si=Si dimer.

The effect of different gaseous molecular precursors and different surfaces on gas-surface reactivity

Our previous work[16] using *partial structural constraint path minimization method* has provided insight into the reaction mechanism for the initial dissociative adsorption of SiH_4 onto a Si(001)-(2×2) surface. Additionally, we also investigated the reaction energy profiles thereby locating the possi-

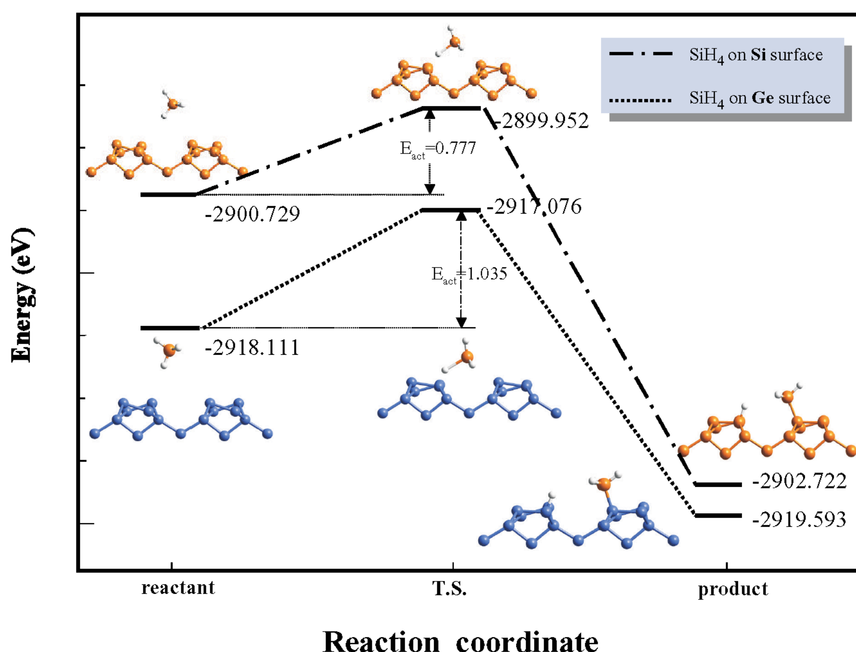

Fig. 2. Energy profile following the partial structural constraint path of the initial dissociative adsorption of SiH_4 onto both Si(001)-(2×2) and Ge(001)-(2×2) surfaces and the corresponding structures. The reaction coordinates refer to the structural constraint of Si-H bond lengths (Å) along the constraint path of the initial dissociative adsorption of SiH_4 onto both Si(001)-(2×2) and Ge(001)-(2×2) surfaces as described in Ref. 16.

ble transition state structure. But how different gaseous molecular precursors and surfaces affect their gas-surface reactivity still remains an open question. Therefore, we will apply the same method to elaborate the effect of different gaseous molecular precursors and different surfaces on their transition state structures and corresponding activation energies. In consequence, we can provide better insight into factors governing their gas-surface reactivity. In this method it is assumed that we already knew the structures of the reactant and the product. Then we propose a constrained path leading from the reactant to the saddle point, and finally to the product. There is no definite way to locate the geometry of the reactant. Therefore, the initial structures of both SiH_4 and GeH_4 at a distance of around 3.60 Å from the H within SiH_4 and GeH_4 to a buckled-down Si/Ge atom on Si(001)-(2×2) and Ge(001)-(2×2) surfaces with both Si-H and Ge-H bond aligned with a surface dangling-bond direction as shown in Fig. 1 and Fig. 2 are used as starting points. These distances are chosen due to the fact that it leads to a very shallow minimum when we allow both SiH_4 and GeH_4 to move toward buckled-down Si/Ge atom with both Si-H and Ge-H bond along the surface dangling-bond direction. Finally, we can proceed with the elongation of Si-H within SiH_4 and Ge-H within GeH_4 and the migration of SiH_3 and GeH_3 leading to the final structures of Si(001)-(2×2)(SiH_3:H and GeH_3:H) and Ge(001)-(2×2)(SiH_3:H and Ge_3H:H), respectively, through the partial structural constraint path as described in one of our previous papers.[16]

To consider the effect of gaseous molecular precursors on the gas-surface reactivity the total energy profiles and corresponding structures of the initial reactant, transition state, and final product for the initial dissociatve adsorption of both SiH_4 and GeH_4 onto Si(001)-(2×2) surface are shown in Fig. 1. Also the calculated structural parameters of the reactants, transition states, and final products are reported in Table 4. These energy barriers using initial reactants as reference states are calculated to be 0.777 eV and 0.533 eV for SiH_4 and GeH_4, respectively. To evaluate their different gas-surface reactivity in a more quantitative way we calculated the ratio of fraction of Boltzmann distribution with sufficient energy to cross these two barriers at the temperature of 700 °C.[13,16] This evaluation includes the ignorance of entropic and dynamic effects and assumes that the gas molecular precursors and surfaces are in equilibrium. This ratio is calculated to be approximately a factor of 18.45, which is nearly three to four times higher than its counterpart (as much as a factor of 5 depending on the incident kinetic energy) derived from measured gas-surface reactivity using supersonic molecular beam techniques.[12] These different gas-surface reactivities can be correlated with other factors such as surface atomic re-

Table 4. (a) Calculated Bond Lengths (Å) and Bond Angles (°) of Reactant (Tr), Transition State (Ts) and Product, and Corresponding Activation Energy E_{act} which is Calculated Approximately as E(Ts)-E(Tr). $R_{Si\text{-}H}$ is the Distance between H within SiH_4 and Buckled-down Si Atom, $R_{Si'\text{-}H}$ is Si-H of SiH_4 and $R_{Si'\text{-}Si''}$ is the Distance between Si within SiH_4 and Buckled-up Si Atom. (b) Calculated Bond Lengths (Å) and Bond Angles (°) of Reactant (Tr), Transition State (Ts) and Product, and Corresponding Activation Energy $E_{act.}$ which is Calculated Approximately as E(Ts)-E(Tr). $R_{Ge\text{-}H}$ is the Distance between H within GeH_4 and Buckled-down Si Atom, $R_{Ge'\text{-}H}$ is Si-H of SiH_4 and $R_{Ge'\text{-}Si''}$ is the Distance between Ge Within GeH_4 and Buckled-up Si Atom. (c) Calculated Bond Lengths (Å) and Bond Angles (°) of Reactant (Tr), Transition State (Ts) and Product, and Corresponding Activation Energy $E_{act.}$ which is Calculated Approximately as E(Ts)-E(Tr). $R_{Ge\text{-}H}$ is the Distance between H within SiH_4 and Buckled-down Ge Atom, $R_{Si'\text{-}H}$ is Si-H of SiH_4 and $R_{Ge'\text{-}Si''}$ is the Distance between Si within SiH_4 and Buckled-up Ge Atom

(a)	Reactant	Transition state	Product
$R_{Si\text{-}H}$(Å)	4.459	1.865	1.491
$R_{Si'\text{-}H}$(Å)	1.483	2.024	3.975
$R_{Si'\text{-}Si''}$(Å)	4.524	3.425	2.303
Si=Si dimer (1) (Å)	2.338	2.443	2.406
Si=Si dimer (2) (Å)	2.318	2.312	2.279
Dimer tilt (1) (°)	18.1	9.7	0.4
Dimer tilt (2) (°)	-15.9	-15.6	-14.0
$E_{act.}$ (eV)			0.777
(b)			
$R_{Si\text{-}H}$(Å)	4.456	1.705	1.491
$R_{Ge'\text{-}H}$(Å)	1.514	2.048	4.209
$R_{Ge'\text{-}Si''}$(Å)	4.687	3.498	2.348
Si=Si dimer (1) (Å)	2.347	2.464	2.370
Si=Si dimer (2) (Å)	2.325	2.280	2.256
Dimer tilt (1) (°)	16.6	6.2	1.3
Dimer tilt (2) (°)	-17.3	-12.2	-14.9
$E_{act.}$ (eV)			0.533
(c)			
$R_{Ge\text{-}H}$(Å)	4.501	1.626	1.529
$R_{Si'\text{-}H}$(Å)	1.477	2.381	4.427
$R_{Si'\text{-}Ge''}$(Å)	6.137	3.698	2.344
Ge=Ge dimer (1) (Å)	2.479	2.568	2.458
Ge=Ge dimer (2) (Å)	2.476	2.409	2.435
Dimer tilt (1) (°)	18.1	8.7	2.1
Dimer tilt (2) (°)	-18.2	-15.3	-17.0
$E_{act.}$ (eV)			1.035

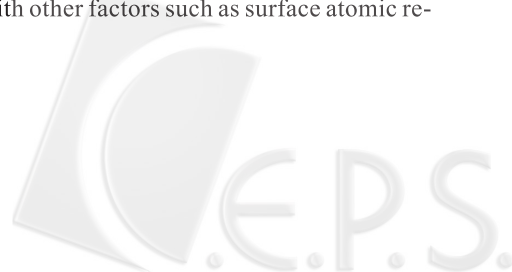

arrangement, internal distortion of gaseous molecular precursor and the different extent of H-Si bond strength, i.e. the H-Si bonds between H within SiH_4/GeH_4 and buckled-down Si atom on Si(001)-(2×2) surface, at their transition states to help us comprehend their different gas-surface reactivities for SiH_4 and GeH_4 initial dissociative adsorption onto the Si(001)-(2×2) surface. Therefore, we will first elaborate on the influence of these structural parameters at their transition states on these calculated energy barriers. Our calculated structural parameters at their transition states for the initial dissociative adsorption of both SiH_4 and GeH_4 onto the Si(001)-(2×2) surface suggest that the elongation of Si-H within SiH_4 and Ge-H within GeH_4 will accompany the unbuckling of buckled Si=Si dimer on Si(001)-(2×2) to give a Si=Si bond length up to 2.443 and 2.464 Å, respectively. They are nearly 0.085 and 0.117 Å longer than the original Si=Si bond length of buckled Si=Si dimer. This indicates that the atomic rearrangement of a buckled Si=Si dimer arising from the variation of surface substrate temperature will be crucial in affecting the reaction profile of SiH_4 and GeH_4 initial dissociative adsorption onto the Si(001)-(2×2) surface. To elaborate on this fact further we realized that as the substrate temperature increases there are more populated vibrational levels for the formation of the $(Si\text{-}H)_{GeH4}$ bond on the Si(001)-(2×2) surface, i.e. 0.117 Å elongation of Si=Si dimer, than those of the $(Si\text{-}H)_{SiH4}$ bond on the Si(001)-(2×2) surface, i.e. 0.085 Å elongation of the Si=Si dimer, provided by the same temperature to reach their transition state. In consequence, there is higher gas-surface reactivity for initial dissociative adsorption of GeH_4 onto the Si(001)-(2×2) surface than that of SiH_4 onto the Si(001)-(2×2) surface. Moreover, we found that the bond length of $(Si\text{-}H)_{SiH4}$, i.e. the distance between H within SiH_4 and the buckled-down Si atom, is 0.160 Å longer than that of $(Si\text{-}H)_{GeH4}$, i.e. the distance between H within GeH_4 and buckled-down Si atom, on Si(001) -(2×2) surface at the transition state. The shorter bond length of $(Si\text{-}H)_{GeH4}$ indicates that the buckled Si=Si dimer participates in a slightly different way to energetically stabilize the transition state, i.e. lower energy barrier, during the formation of $(Si\text{-}H)_{GeH4}$ bond on Si(001)-(2×2) surface.

Now we will consider the effect of different surfaces, i.e. Si(001)-(2×2) and Ge(001)-(2×2), on the gas-surface reactivity for the initial dissociative adsorption of GeH_4 onto these surfaces. Again only the total energy profiles and corresponding structures of the initial reactant, transition state, and final product for the initial dissociatve adsorption of both GeH_4 onto both Si(001)-(2×2) and Ge(002)-(2×2) surfaces are shown in Fig. 2. Also the calculated structural parameters of the reactants, transition states, and final products are reported in Table 4. These energy barriers using initial reactants as reference states are calculated to be 0.777 eV and 1.035 eV for Si(001)-(2×2) and Ge(002)-(2×2), respectively. To evaluate their different gas-surface reactivity in a more quantitative way we calculated the ratio of fraction of Boltzmann distribution with sufficient energy to cross these two barriers at the temperature of 700 °C.[13,16] This ratio is calculated to be approximately a factor of 21.69, which is only two times higher than its counterpart (approximately a factor of 10 depending on the incident kinetic energy) derived from measured gas-surface reactivity using supersonic molecular beam techniques.[12] To appreciate the effect of different surfaces, i.e. Si(001)-(2×2) and Ge(001)-(2×2), on the gas-surface reactivity for initial dissociative adsorption of SiH_4 onto these surfaces we again correlate their calculated structural parameters at their transition states with their corresponding activation energies in order to gain better insight into the factors governing their gas-surface reactivity. We can easily find from our calculated structural parameters that as the elongation of Si-H proceeds to form the transition state on both Si(001)-(2×2) and Ge(001)-(2×2) surfaces the bond length of Si-H within SiH_4 on Si(001)-(2×2) is nearly 0.36 Å longer than that of Si-H within SiH_4 on Ge(001)-(2×2). Consequently, there is less energy needed to reach the transition state on the Ge(001)-(2×2) surface. On the other hand, the bond length of Ge-H between H within SiH_4 and buckled-up Ge atom on Ge(001)-(2×2) surface is about 0.24 Å shorter than that of Si-H between H within SiH_4 and a buckled-up Si atom on a Si(001)-(2×2) surface. But the nature of a weaker bond of Ge-H on Ge(001)-(2×2) surface seems to compensate for less energy than is needed to stabilize its transition state in comparison with that of the stronger bond of Si-H on the Si(001)-(2×2) surface. In summary, the forming of a stronger bond of Si-H between H within GeH_4 and a buckled-down Si atom on a Si(001)-(2×2) surface and the less internal distortion of a Ge-H bond within gaseous molecular precursor of GeH_4 at the transition state are two main factors causing the different gas-surface reactivities for the initial dissociative adsorption of both GeH_4 and SiH_4 onto a Si(001)-(2×2) surface. Also the less internal distortion of Si-H within the gaseous molecular precursor of SiH_4 and the different nature of Ge-H and Si-H bonds between the gaseous molecular precursor of SiH_4 and Si(001)-(2×2)/Ge(001)-(2×2) surfaces are two of the major factors to affect their gas-surface reactivity for the initial dissociative adsorption of SiH_4 onto both

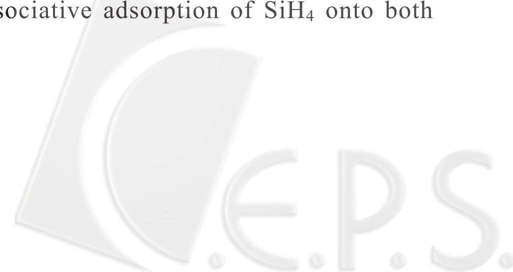

Si(001)-(2×2) and Ge(001)-(2×2) surfaces.

CONCLUSIONS

By combining total energy calculations based on DFT with GGA and ultrasoft pseudopotential approximation we have successfully established the energetic profile for the initial dissociative adsorption of silane (SiH_4) and germane (GeH_4) onto both Si(001)-(2×2) and Ge(001)-(2×2) surfaces to evaluate the effect of different gaseous molecular precursors and different surfaces on their gas-surface reactivity for this process. Our calculated results are summarized below. Firstly, the better evaluated gas-surface reactivity for the initial dissociative adsorption of GeH_4 onto the Si(001)-(2×2) surface than that for the initial dissociative adsorption of SiH_4 onto Si(001)-(2×2) surface, i.e. approximately a factor of 18.45, is nearly three to four times higher than experimentally measured gas-surface reactivity using supersonic molecular beam techniques. And we attributed its better evaluated gas-surface reactivity to the forming of the stronger bond of H-Si between H within GeH_4 and buckled-down Si atom on a Si(001)-(2×2) surface and the less internal distortion of Ge-H within GeH_4 at the transition state to lower its energy barrier. Secondly, our better evaluated gas-surface reactivity for the initial dissociative adsorption of SiH_4 onto a Si(001)-(2×2) surface than that for the initial dissociative adsorption of SiH_4 onto a Ge(001)-(2×2) surface, i.e. approximately a factor of 21.69, is only two times higher than the experimental data. And we believe that this better evaluated gas-surface reactivity is due to the less internal distortion of Si-H within the gaseous molecular precursor of SiH_4 and the different nature of Ge-H and Si-H bonds between the gaseous molecular precursor of SiH_4 and Si(001)-(2×2)/Ge(001)-(2×2) surfaces at their transition states.

ACKNOWLEDGMENTS

The authors would like to thank the National Science Council in Taiwan for financial support (Grant No. 90-2113-M-032-006 and 91-2113-M-032-006) and the use of computational facilities from the National Center for High Performance Computing and Tamkang University in Taiwan.

Received December 23, 2002.

REFERENCES

1. Mokler, S. M. *Crit. Rev. Surf. Chem.* **1994**, *4*, 1.
2. Bean, J. C. *Proc. IEEE* **1992**, *80*, 571.
3. Meyerson, B. S. *IBM J. Res. Dev.* **1990**, *34*, 806.
4. Gates, S. M. *Surf. Sci.* **1988**, *195*, 307.
5. Gates, S. M.; Greenlief, C. M.; Beach, D. B.; Kunz, R. R. *Chem. Phys. Lett.* **1989**, *154*, 505.
6. Gates, S. M.; Greenlief, C. M.; Beach, D. B. *J. Chem. Phys.* **1990**, *93*, 7493.
7. Gates, S. M.; Greenlief, C. M.; Beach, D. B.; Holbert, P. A. *J. Chem Phys.* **1990**, *92*, 3144.
8. Gates, S. M.; Greenlief, C. M.; Kulkarni, S. K.; Sawin, H. H. *J. Vac. Sci. Technol. A* **1990**, *8*, 2965.
9. Gates, S. M.; Kulkarni, S. K. *Appl. Phys. Lett.* **1991**, *58*, 2963.
10. Jones, M. E.; Xia, L.-Q.; Maity, N. J.; Engstrom, R. *Chem. Phys. Lett.* **1994**, *229*, 401.
11. Xia, L.-Q.; Jones, M. E.; Maity, N.; Engstrom, J. R. *J. Vac. Sci. Technol. A.* **1995**, *13*, 2651.
12. Lam, A. M.; Zheng, Y.-J.; Engstrom, J. R. *Surf. Sci.* **1997**, *393*, 205.
13. Brown, A. B.; Doren, D. J. *J. Chem. Phys.* **1999**, *110*, 2643.
14. Jing, Ze; Whitten, J. L. *Phys. Rev.* B **1990**, *44*, 1741.
15. Lin, J. S.; Kuo, Y. T.; Lee, M. H.; Lee, K. H.; Chen, J. C. *J. Mol. Structure: THEOCHEM* **2000**, *496*, 163.
16. Lin, J. S.; Kuo, Y. T. *Thin Solid Films* **2000**, *370*, 192.
17. Parr, R. G.; Yang, W. *Density-Functional Theory of Atoms and Molecules*; Oxford University Press: New York, 1989.
18. Ihm, J. *Rep. Prog. Phys,* **1988**, *51*, 105.
19. Payne, M. C.; Teter, M. P.; Allan, D. C.; Arias, T. A.; Joannopoulos, J. D. *Rev. Mod. Phys*. **1992**, *64*, 1045.
20. Teter, M. P.; Payne, M. C.; Allan, D. C. *Phys. Rev.* B **1989**, *40*, 12255.
21. Kresse, G.; Furthmuller, J. *Computational Materials Science 6*, **1996**, *6*, 15.
22. Perdew, J. P.; Wang, Y. *Physical Rev. B* **1992**, *45*, 13244.
23. White, J. A.; Bird, D. A. *Physical Rev. B* **1994**, *50*, 4954.
24. Monkhorst, H. J.; Pack, J. D. *Phys. Rev. B* **1976**, *13*, 5188.
25. Kerker, G. *J. Phys. C.* **1980**, *13*, L189.
26. Hamann, D. R.; Schluter, M.; Chiang, C. *Phys. Rev. Lett.* **1979**, *43*, 1494.
27. Bachelet, G. B.; Hamann, D. R.; Schluter, M. *Phys. Rev. B* **1982**, *26*, 4199.
28. Vanderbilt, D. *Phys. Rev. B* **1990**, *41*, 7892.
29. Kleinman, L.; Bylander, D. M. *Phys. Rev. Lett.* **1982**, *48*, 1425.
30. Lin, J. S.; Qteish, A.; Payne, M. C.; Heine, V. *Phys. Rev. B* **1993**, *47*, 4174.
31. Lin, J. S.; Payne, M. C.; Heine, V.; McConnell, J. D. C. *Phys. Chem. Minerals* **1994**, *21*, 150.
32. Stich, I.; Payne, M. C.; King-Smith, R. D.; Lin, J. S.; Clarke,

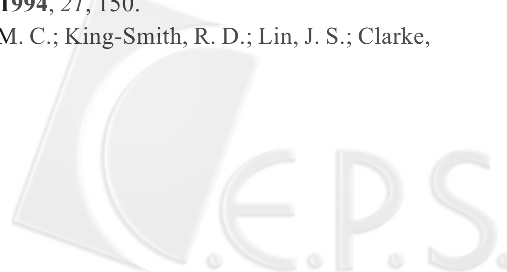

L. J. *Phys. Rev. Lett.* **1992**, *68*, 1351.
33. CASTEP, 3.9 ed. (Molecular Simulations, Inc., 1999).
34. Walsh, R. *Acc. Chem. Res.* **1981**, *14*, 246.
35. Kresse, G.; Hafner, J. *J. Phys. Condens. Matter* **1984**, *6*, 8245.
36. Kang, J. K.; Musgrave, C. B. *Phys. Rev. B* **2001**, *64*, 245330.
37. Katircioglu, S.; Erkoc, S. *Surf. Rev. Lett.* **2002**, *9*, 1401.
38. Lin, J. S.; Kuo, Y. T.; Chen, J. C.; Lee, M. H. *J. Chin. Chem. Soc*. **2000**, *47*, 887.
39. Srivastava, G. P. *Rep. Prog. Phys.* **1997**, *60*, 561.
40. Miotto, R.; Ferraz, A. C. *Surface Science* **2002**, *513*, 422.